





Cite this: *New J. Chem.*, 2023, 47, 192

Continuous and large-scale synthesis of Ni–Co PBA nanoparticles with a tunable particle size in a microreactor†

Huanhuan Wang, Qi Qu, Zhiming Liu,  Yan He * and Jiangshan Gao*

Herein, we report a micro-mix strategy for the continuous and large-scale synthesis of Ni–Co PBA nanoparticles. The technique presented in this study allows the particle size to be controlled in the 165 nm to 350 nm range while maintaining a high specific surface area ($250 \text{ m}^2 \text{ g}^{-1}$) and cubic structure. Furthermore, the particles exhibit superior dispersity and have a more homogeneous particle size than those prepared using the conventional stirring-mix method due to the drastic collisions that occur in the microchannel during the precipitation process. The present study demonstrates that the concentration of raw materials and feed flow rates in the microreactor effectively control the particle size during mixing. The high concentration of raw materials could decrease the particle size, and the particle size is decreased with the increasing feed flow rates when Re (Reynolds number) < 783 . Particularly, when $783 < Re < 1567$, the particle size remains stable (about $165 \pm 10 \text{ nm}$). Additionally, the space-time yield (STY) of Ni–Co PBA is $471 \text{ kg m}^{-3} \text{ d}^{-1}$. Finally, the continuous flow microreactor can continuously fabricate large-scale and high-quality Ni–Co PBA crystals with distinct morphological features in a short period of time, providing an effective alternative to the time-consuming and multi-step MOF synthesis method.

Received 2nd September 2022,
Accepted 17th November 2022

DOI: 10.1039/d2nj04385h

rsc.li/njc

1. Introduction

In recent years, metal–organic frameworks (MOFs) have become a temporal requirement due to the constant demand for novel porous materials. They have attracted much attention due to their extremely diverse structural topologies and tunable chemical properties.¹ Prussian blue analogues (PBAs) have broad application prospects as a kind of MOF with special structures and unique physicochemical properties.^{2,3} Recently, Ni–Co PBA nanocubes have been used as self-sacrificial precursors to synthesize composites with excellent electrochemical performance, electrocatalytic activity, and microwave absorption. For example, Yi *et al.*⁴ reported a simple template-intercalation strategy to synthesize well-defined cubic quasi-hollow nickel–cobalt phosphides using Ni–Co PBA nanocubes as self-sacrificial precursors. Among the metal phosphides synthesized with different

compositions, the almost hollow Ni–Co nano-cubic phosphide exhibits the best electrocatalytic activity. Yu *et al.*⁵ reported Ni–Co-doped MoS_2 nanoboxes synthesized by the reaction of Ni–Co PBA nanobatteries with ammonium thiomolybdate. The well-defined Ni-doped and Co-doped MoS_2 nanoboxes exhibit excellent electrochemical activity as electrocatalysts for the hydrogen evolution reaction. Gao *et al.*⁶ described the construction of $\text{MnO}_2/\text{Mn}_3\text{O}_4@ \text{Ni-Co/GC}$ nanocubes with porous structures and ultrathin nanosheets by self-modeling and *in situ* synthesis strategies, which exhibited excellent electromagnetic absorption properties. Controlling of agglomeration of PBAs is fundamental to be exploited in diverse application-based fields such as catalysis,⁷ energy storage,^{8–10} chemical sensing,¹¹ gas storage, separation,¹² *etc.* Traditional methods such as hydrothermal, solvothermal or stirring-mix methods for synthesizing MOFs are time-consuming.¹³ These methods take hours or days to crystallize and form a porous network. In addition, the samples prepared by traditional methods have inferior dispersion and are low-yielding, causing inconvenience to subsequent applications.^{14–16} Conventional techniques cannot meet the requirements of large-scale production due to batch-to-batch variability.^{17–20}

Recently, the continuous flow microreactor technology has been shown to be an efficient synthesis method.^{21–25} Compared with the traditional stirring-mix method, microreactors have

College of Electromechanical Engineering, Shandong Engineering Laboratory for Preparation and Application of High-performance Carbon Materials, Qingdao University of Science and Technology, Qingdao 266061, China.

E-mail: heyang@qust.edu.cn, gaojs@qust.edu.cn

† Electronic supplementary information (ESI) available: Detailed parameters for the preparation of Ni–Co PBA particles via the conventional stirring-mix method (Table S1) and microreactor technology (Table S2). Physical pore parameters of Ni–Co PBA particles produced at different feed flow rates (Table S3–S5). See DOI: <https://doi.org/10.1039/d2nj04385h>

higher surface area-to-volume ratios and shorter characteristic transport paths, which ensure efficient heat and mass transfer rates and excellent mixing capabilities.^{26–28} These are key factors for the nucleation and growth of nanoparticles. Furthermore, the small volume of the reactor means safer operation and less waste compared to the traditional stirring-mix method.^{29,30} Since it is a continuous flow reaction, it paves the way for possible large-scale production. For example, Tai *et al.*³¹ reported a facile method for producing size-tunable UiO-66 nanoparticles in a continuous flow microreactor. Zhang *et al.*³² synthesized ZIF-67 at ambient temperature and pressure with the microfluidic strategy. Poly-zoidis *et al.*³³ synthesized UiO-66 continuously by employing microreactors and the concept of flow chemistry. Ayumi *et al.*³⁴ designed a combinatorial system for the synthesis of CdSe nanoparticles using the parallel operation of microreactors. These explorations demonstrate the synthetic efficiency of microreactor systems.

A microreactor provides a uniform reaction field for solution mixing and realizes rapid and uniform mixing of the solution. During the experiment, the diffusion of molecules plays a dominant role in microspace. In addition, rapid heat control is achieved due to the increased heat transfer area.³⁵ Theoretically, the molecular diffusion time scale (t) is proportional to the square of the characteristic heat conduction distance (L), i.e. $t \propto L^2$. The synthesis of particles consists of three steps: (1) increasing the product concentration, (2) rapid nucleation, and (3) particle growth. The microreactor has good mixing and heat transfer properties, which can control the nucleation process and particle growth process.

In this work, we propose a strategy for the production of Ni-Co PBA particles in a microreactor, which can be regarded as an important platform for the production of size-tunable Ni-Co PBA particles. The experimental setup for the continuous synthesis of Ni-Co PBA is shown in Scheme 1. We examine the consequences of different concentrations of raw materials and feed flow rates on particle size and crystal morphology *via*

varying the process parameters. Furthermore, the impacts of the conventional stirring-mix method and continuous flow microreactor technology on the particle size, crystallization status and dispersion of Ni-Co PBA are also compared. Finally, the particle size of Ni-Co PBA can be controlled between 165 nm and 350 nm by simply controlling the reaction conditions.

2. Methods and experiments

2.1 Materials

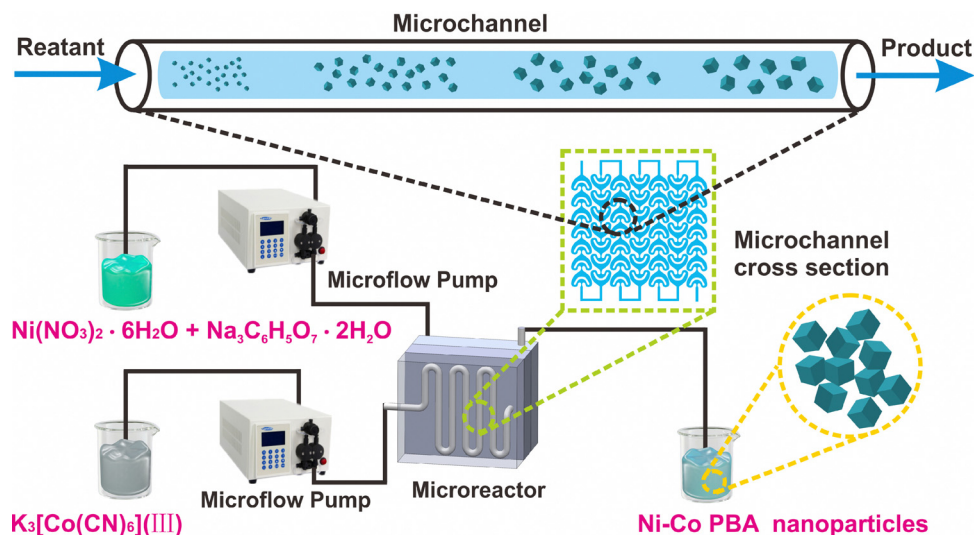
$\text{Ni}(\text{NO}_3)_2 \cdot 6\text{H}_2\text{O}$, $\text{Na}_3\text{C}_6\text{H}_5\text{O}_7 \cdot 2\text{H}_2\text{O}$ and $\text{K}_3[\text{Co}(\text{CN})_6](\text{III})$ were acquired from Shanghai Aladdin Reagent Corporation. All reagents were of analytical grade and can be used without factitious treatment.

2.2 Synthesis of Ni-Co PBA

Synthesis of Ni-Co PBA nanoparticles using the conventional stirring-mix method:³⁶

A mixed solution of 1.8/3.6/5.4 mmol $\text{Ni}(\text{NO}_3)_2 \cdot 6\text{H}_2\text{O}$, 2.7/5.4/8.1 mmol $\text{Na}_3\text{C}_6\text{H}_5\text{O}_7 \cdot 2\text{H}_2\text{O}$ and 60 mL deionized (DI) water was added to another solution containing 1.2/2.4/3.6 mmol $\text{K}_3[\text{Co}(\text{CN})_6](\text{III})$ and 60 mL of DI water. The obtained solution was magnetically stirred for 1 minute and left at room temperature for 24 hours. After washing with DI water and absolute ethanol, Ni-Co PBA was obtained. The particles prepared at various concentrations were named Ni-Co PBA-1#, Ni-Co PBA-2# and Ni-Co PBA-3#. The detailed parameters for the preparation of Ni-Co PBA particles *via* the conventional stirring-mix method are listed in Table S1 (ESI†).

Synthesis of Ni-Co PBA nanoparticles in a continuous flow microreactor: Solution A was made up of 1.8/3.6/5.4 mmol $\text{Ni}(\text{NO}_3)_2 \cdot 6\text{H}_2\text{O}$ and 2.7/5.4/8.1 mmol sodium citrate with 60 mL of DI water. Solution B was made up of 1.2/2.4/3.6 mmol $\text{K}_3[\text{Co}(\text{CN})_6](\text{III})$ with 60 mL of DI water. Solution A and solution B were pumped into a microreactor at room temperature by two



Scheme 1 Schematic diagram of the experimental set-up for the continuous synthesis of Ni-Co PBA.

microfluidic pumps at the same feed rate, and the suspension was collected at the outlet of the microchannel. The obtained suspension was washed with DI water and absolute ethanol, respectively, and dried in a vacuum drying oven to obtain the solid powder, named Ni-Co PBA-1#-X, Ni-Co PBA-2#-X and Ni-Co PBA-3#-X ($X = 2, 4, 6, 8, 10, 12, 14$ and 16 mL min^{-1}). The symbol 'X' represented different feed flow rates. The feed flow rates for the overall reaction ranged from 2 to 40 mL min^{-1} , and the experimental temperature and pressure ranges were 25°C and 0–10 MPa, respectively. The detailed parameters for the preparation of Ni-Co PBA particles in a microreactor are listed in Table S2 (ESI†).

2.3 Characterization

The scanning electron microscopy (SEM) images are obtained using a HITACHI SU8010 SEM. The composition of the product is recorded by X-ray powder analysis (XRD) (Rigaku MiniFlex600). Fourier transform infrared spectroscopy (FTIR) is recorded using a Nicolet iS50 FT-IR spectrometer at a wavelength of $400\text{--}4000 \text{ cm}^{-1}$. The surface area is calculated according to the Brunauer–Emmett–Teller (BET) method using N_2 adsorption data at 77 K. The particle size distribution of the resultant Ni-Co PBA dispersed in DI water is measured by dynamic light scattering (DLS) using a Laser particle sizer (LPS, Brookhaven Instruments Ltd., US).

3. Results and discussion

Continuous synthesis of Ni-Co PBA nanoparticles is first investigated. The experiments begin with an in-depth investigation

of the consequences of different reaction parameters in the continuous flow microreactor. At room temperature, Ni-Co PBA is synthesized by the conventional stirring-mix method and continuous flow microreactor technology, respectively. In the first set of experiments, the amounts of the substance of $\text{Ni}(\text{NO}_3)_2 \cdot 6\text{H}_2\text{O}$, sodium citrate and $\text{K}_3[\text{Co}(\text{CN})_6](\text{III})$ are 1.8 mmol, 2.7 mmol and 1.2 mmol, respectively. As shown in Scheme 1, $\text{Ni}(\text{NO}_3)_2 \cdot 6\text{H}_2\text{O}$, sodium citrate and $\text{K}_3[\text{Co}(\text{CN})_6](\text{III})$ aqueous solutions are transported to the microreactors in the same feed flow rate through a microflow pump. The two aqueous solutions are mixed in an umbrella-type mixer and then seed aggregates are formed in microchannels. These seeds agglomerate to form small-sized Ni-Co PBA particles that further grow in the process of static precipitation. Fig. 1 exhibits the SEM images of Ni-Co PBA particles synthesized at different feed flow rates (2, 4, 6, 8, 10, 12, 14, 16 mL min^{-1}). According to SEM images (Fig. 1(a)), the particle size of Ni-Co PBA prepared by the conventional stirring-mix method is about $250 \pm 15 \text{ nm}$. As shown in Fig. 1(b)–(i), Ni-Co PBA particles synthesized at different feed flow rates have excellent quality and stable regular tetrahedron morphology. When the feed flow rate is 2, 4, 6, 8, 10, 12, 14 and 16 mL min^{-1} , the particle size of Ni-Co PBA is 193 ± 12 , 249 ± 14 , 226 ± 12 , 259 ± 16 , 262 ± 13 , 316 ± 14 , 312 ± 11 and $305 \pm 14 \text{ nm}$, respectively. That is to say, the particle size of Ni-Co PBA shows a tendency to first increase and then decrease with the increased feed flow rate.

In the second set of experiments, the impact of different raw material concentrations on particle size and dispersion is

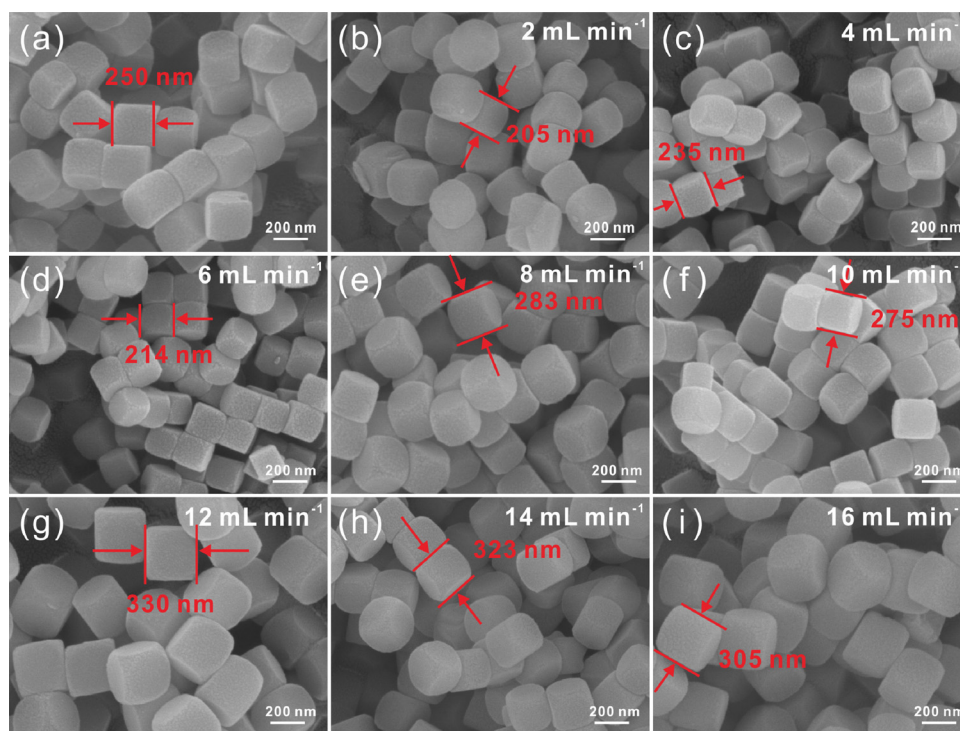


Fig. 1 SEM images of Ni-Co PBA-1# nanoparticles. (a) Ni-Co PBA nanoparticles prepared by the conventional stirring-mix method; Ni-Co PBA nanoparticles obtained at feed flow rates of (b) 2 mL min^{-1} , (c) 4 mL min^{-1} , (d) 6 mL min^{-1} , (e) 8 mL min^{-1} , (f) 10 mL min^{-1} , (g) 12 mL min^{-1} , (h) 14 mL min^{-1} and (i) 16 mL min^{-1} in a microreactor.

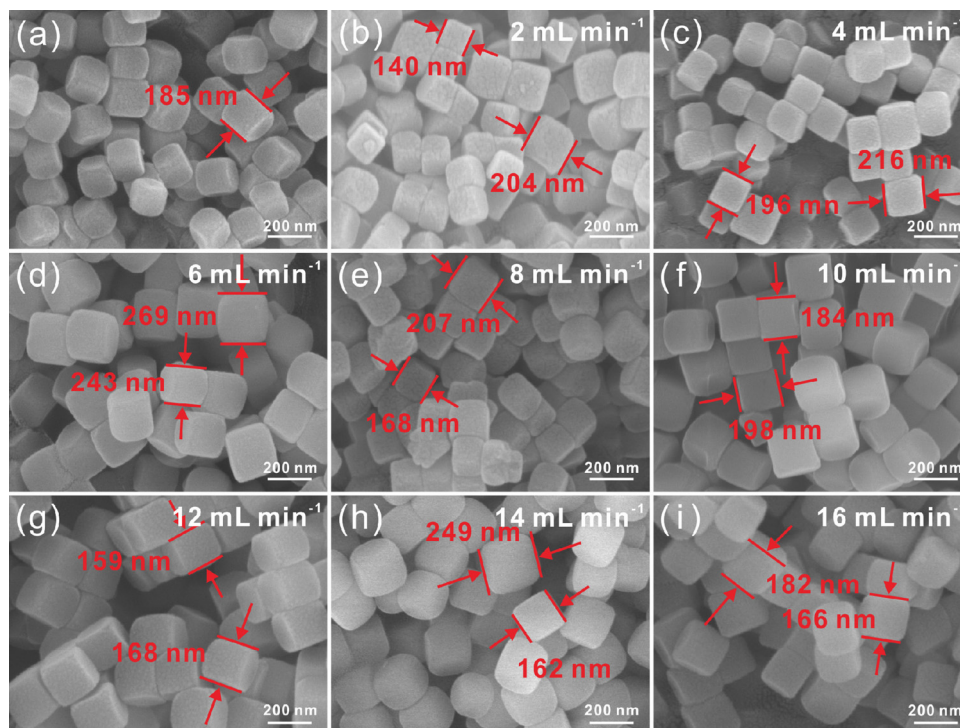


Fig. 2 SEM images of Ni-Co PBA-2# nanoparticles. (a) Ni-Co PBA nanoparticles prepared by the conventional stirring-mix method; Ni-Co PBA nanoparticles obtained at feed flow rates of (b) 2 mL min⁻¹, (c) 4 mL min⁻¹, (d) 6 mL min⁻¹, (e) 8 mL min⁻¹, (f) 10 mL min⁻¹, (g) 12 mL min⁻¹, (h) 14 mL min⁻¹ and (i) 16 mL min⁻¹ in a microreactor.

investigated. The amount of substance of Ni(NO₃)₂·6H₂O, sodium citrate and K₃[Co(CN)₆](III) is varied as 3.6 mmol, 5.4 mmol and 2.4 mmol, respectively. According to SEM images (Fig. 2(a)), the particle size of Ni-Co PBA prepared by the conventional stirring-mix method is about 185 ± 10 nm. Compared with the first set of experiments, the particle size decreases when the concentration of raw materials increases. Fig. 2(b)–(i) show the SEM images in the cases of feed flow rates of 2, 4, 6, 8, 10, 12, 14 and 16 mL min⁻¹, respectively. As the feed flow rate increases, the particle size becomes small and still maintains the shape of a regular tetrahedron shape. Particularly, with shorter reaction times (aging times), less time is given for crystal growth and thus smaller crystals are produced. Meanwhile, the particle size of Ni-Co PBA becomes homogeneous with the increase of feed flow rates. The experimental result further indicates that the particle size and uniformity of Ni-Co PBA particles can be regulated by changing the feed flow rate.

In the third set of experiments, the amount of substance of Ni(NO₃)₂·6H₂O, sodium citrate and K₃[Co(CN)₆](III) is varied as 5.4 mmol, 8.1 mmol and 3.6 mmol, respectively. It should be noted that the concentration of raw materials has only little impact on the morphology of Ni-Co PBA particles. Meanwhile, it has a great impact on particle size and uniformity. Moreover, at low feed flow rates (2, 4 mL min⁻¹), a bit of small-sized Ni-Co PBA particles exist on the surface of the largest ones. On the other hand, under the condition of high raw material concentrations, more nuclei are formed due to the high degree of

supersaturation, so the particle size of Ni-Co PBA is small^{37,38} (Fig. (3)). Most of the samples are composed of particles with uneven sizes, and larger particles co-exist with much smaller ones. This probably originates from a heterogeneous nucleation of crystals at the surface of existing ones. This phenomenon is particularly evident in the fourth set of experiments (Fig. S1, ESI†). In summary, the four sets of experiments demonstrate that the particle size can be readily controlled by moving the feed flow rate and the concentration of raw materials in microreactors.

Fig. 4 exhibits the XRD patterns of Ni-Co PBA particles synthesized by the conventional stirring-mix method and continuous flow microreactor technology. It can be clearly seen that the diffraction peak of Ni-Co PBA (JCPDS card No. 89-3738) at 17.5°, 24.8°, 35.4°, and 39.7° is attributed to the (200), (220), (400) and (420) plane, respectively. Besides, the shrill peak shape indicates that Ni-Co PBA has a complete nanocubes structure. Meanwhile, the XRD patterns of Ni-Co PBA synthesized at various feed flow rates agree fairly well with the XRD pattern of Ni-Co PBA synthesized by the conventional stirring-mix method, proving the successful formation of Ni-Co PBA particles. The well-defined peaks indicate that the microreactor technology produces particles with high crystallinity and no detectable impurities.

The FT-IR spectroscopy is conducted and the results are shown in Fig. 5(a)–(c). According to the infrared absorption frequency table, the peaks at 1417.2 and 2187.8 cm⁻¹ could be corresponding to the stretching vibration of –CH, and –CN of Ni-Co PBA. Moreover, the peak at 3647.7 cm⁻¹ is assigned to

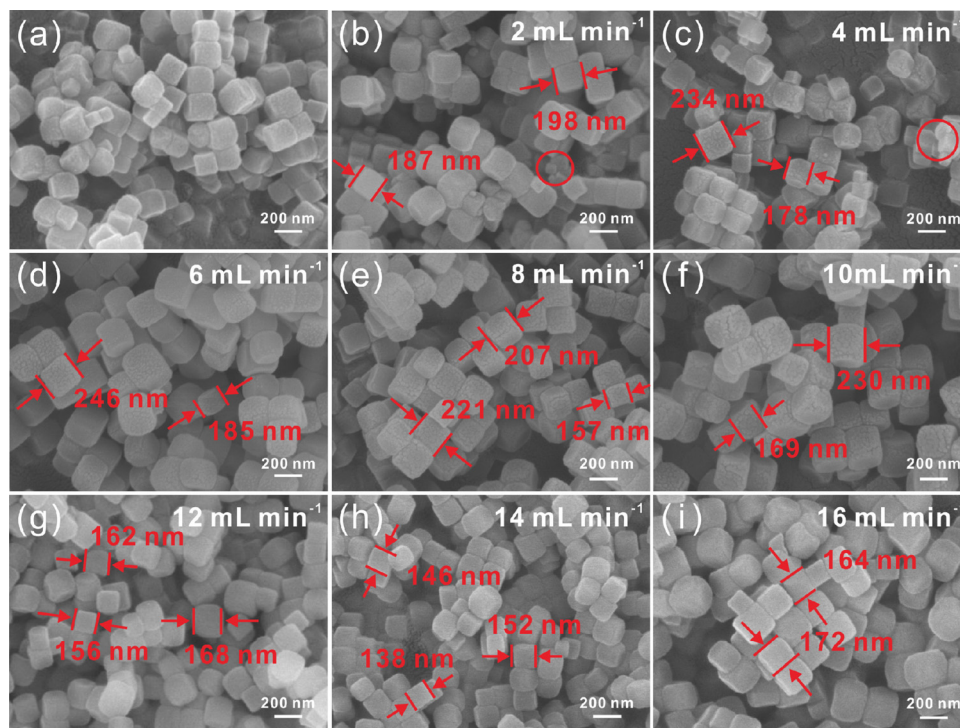


Fig. 3 SEM images of Ni-Co PBA-3# nanoparticles. (a) Ni-Co PBA nanoparticles prepared at the conventional stirring-mix method; Ni-Co PBA nanoparticles obtained at feed flow rates of (b) 2 mL min⁻¹, (c) 4 mL min⁻¹, (d) 6 mL min⁻¹, (e) 8 mL min⁻¹, (f) 10 mL min⁻¹, (g) 12 mL min⁻¹, (h) 14 mL min⁻¹ and (i) 16 mL min⁻¹ in a microreactor.

the O–H stretching and bending modes of water. The peaks are consistent with the peaks of Ni-Co PBA crystals produced using the conventional stirring-mix method, indicating that Ni-Co PBA synthesized in a microreactor does not affect particle crystallinity. The clear peaks indicate that the particles fabricated using a microreactor have a high degree of crystallinity with no detectable impurities. Therefore, the FT-IR spectra further confirm the formation of the product.

Fig. 6 shows the consequences of raw materials concentration and feed flow rates on the particle size of Ni-Co PBA particles. It can be clearly seen that particle size is significantly correlated with feed flow rates and raw material concentration. As shown in Fig. 6(a–c), the particle size of Ni-Co PBA-1#-X, Ni-Co PBA-2#-X, and Ni-Co PBA-3#-X shows a tendency of increasing first and then decreasing with the increase in the feed flow rate. Additionally, when the feed flow rate keeps consistent, the higher the concentration of raw materials, the more obvious the trend of particle size reduction.

The light-intensity distributions of the Ni-Co PBA particles prepared in a microreactor further demonstrate the above conclusion. At the same feed flow rate, Ni-Co PBA synthesized using a microreactor has a narrow size distribution with the increase in the concentration of raw materials as shown in Fig. 7. In addition, Ni-Co PBA particles also have a narrow size distribution with the increase of feed flow rate under the same concentration of raw materials. This may be due to transient nucleation during mixing, leading to particle growth during rapid and uniform mixing in the microreactor.^{39–41} These results

demonstrate that the synergistic effect of raw materials concentration and feed flow rates have a certain degree of influence on the particle size distribution of Ni-Co PBA.

Furthermore, the N₂ adsorption/desorption isotherms of Ni-Co PBA synthesized under different conditions at 77.3 K are shown in Fig. 8. The pore size distributions are determined using the Horvath–Kawazoe method.^{42,43} Fig. 8(a) shows the N₂ adsorption/desorption isotherms of Ni-Co PBA-1#-2#-3# particles synthesized *via* the conventional stirring-mix method. As shown in Table 1, the BET surface area of Ni-Co PBA-1#-2#-3# is 77.36, 95.04 and 93.33 m² g⁻¹, respectively. In addition, Ni-Co PBA particles synthesized through the continuous flow microreactor technology with large differences in particle size are also selected for BET measurements. Fig. 8(b)–(d) shows the N₂ adsorption/desorption isotherms of Ni-Co PBA particles when the feed flow rate is 2, 6, 10 and 14 mL min⁻¹ for the three reaction concentrations. It is obvious that the specific surface area gradually increases and the adsorption behavior is improved in the region of $P/P_0 > 0.95$. The BET surface area of Ni-Co PBA-3# particles prepared in a continuous flow microreactor is 113.76, 139.34, 226.32 and 250.05 m² g⁻¹, respectively, which are much higher than that of Ni-Co PBA prepared by the stirring-mix method reported in the literature (32.90 m² g⁻¹).⁴⁴ It is worthy of note that the Ni-Co PBA particles synthesized through a continuous flow microreactor technology exhibit excellent specific surface areas and micropore volumes compared to the particles produced by the conventional stirring-mix method, further highlighting their

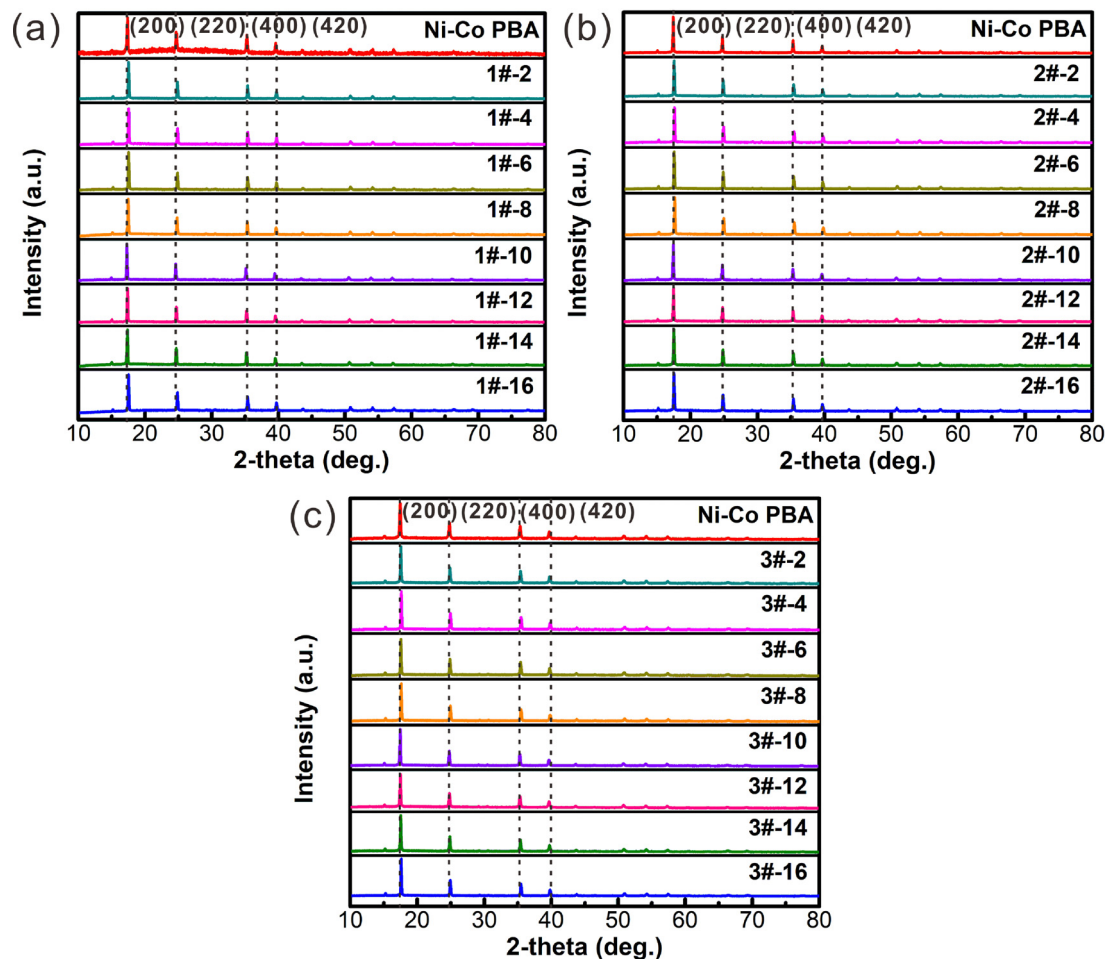


Fig. 4 Measured XRD patterns (a–c) of Ni–Co PBA particles with various feed flow rates and compared with the XRD pattern of Ni–Co PBA prepared by the conventional stirring-mix method.

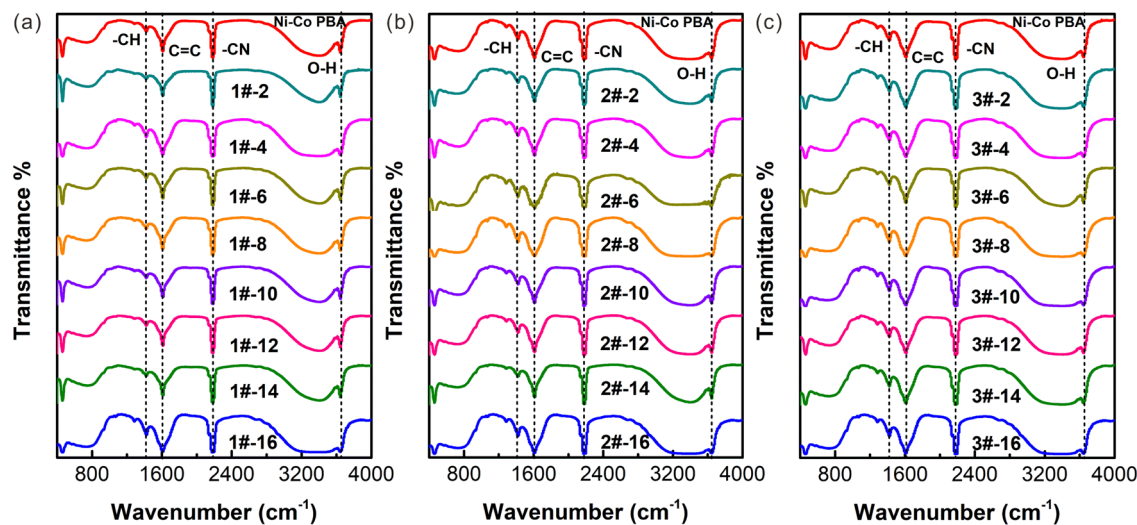


Fig. 5 Measured FT-IR spectra (a–c) of Ni–Co PBA particles with various feed flow rates and compared with the FT-IR spectra of Ni–Co PBA prepared by the conventional stirring-mix reaction.

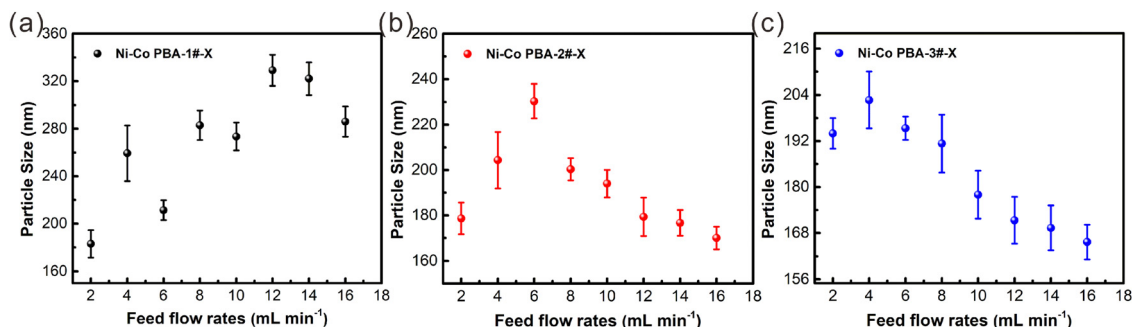


Fig. 6 The particle sizes of (a) Ni-Co PBA-1#-X, (b) Ni-Co PBA-2#-X, and (c) Ni-Co PBA-3#-X ($X = 2, 4, 6, 8, 10, 12, 14$ and 16 mL min^{-1}) at different feed flow rates. Error bars indicate the standard deviation of the data.

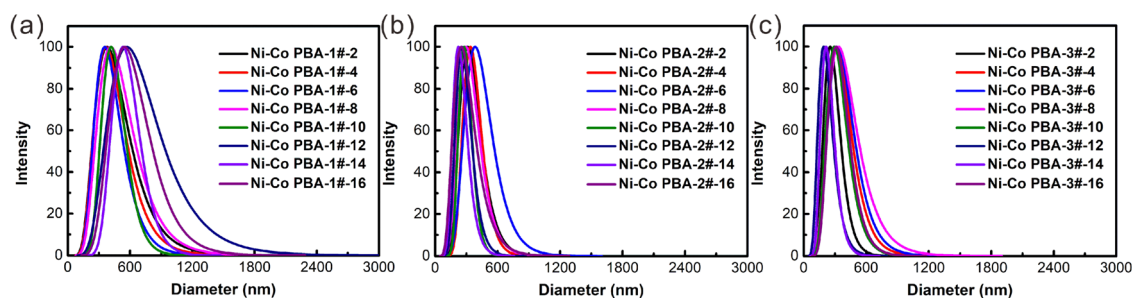


Fig. 7 Light-intensity distributions of the Ni-Co PBA particles prepared in the microreactor. Measurements are conducted using the DLS principle.

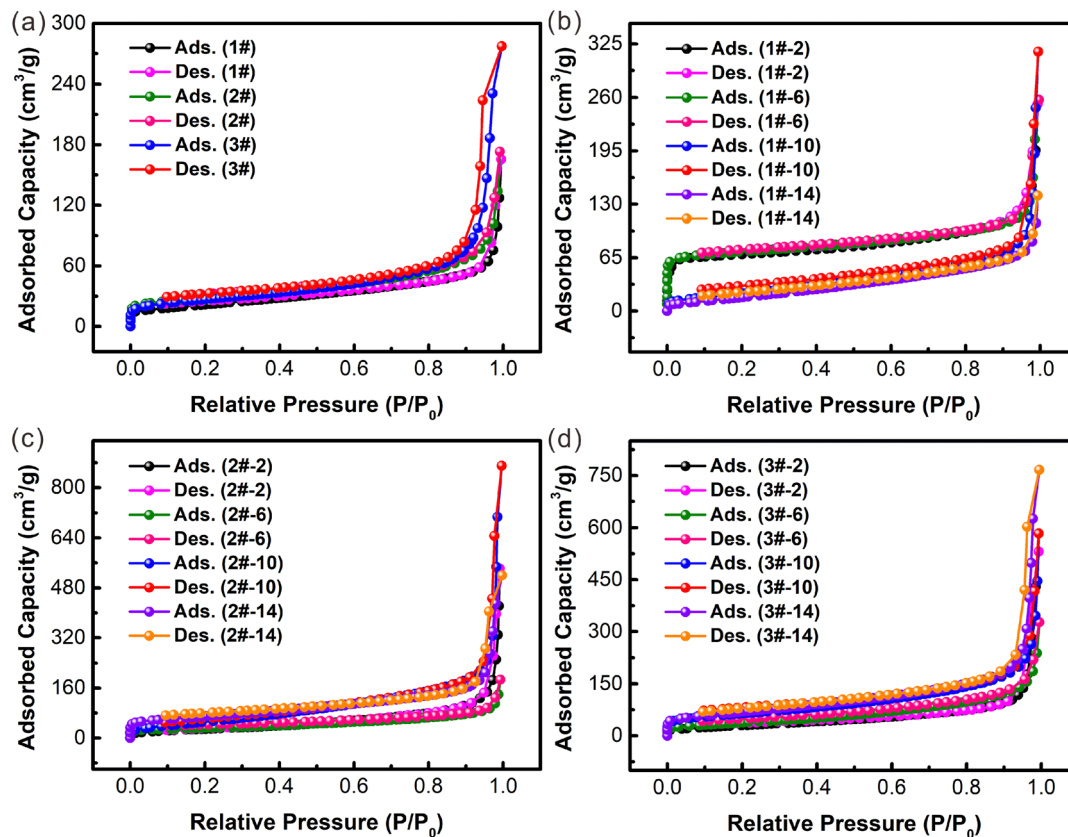


Fig. 8 Nitrogen sorption isotherms of (a) Ni-Co PBA-1#, 2#, 3#; (b) Ni-Co PBA-1#-X, (c) Ni-Co PBA-2#-X and (d) Ni-Co PBA-3#-X crystals ($X = 2, 6, 10, 14 \text{ mL min}^{-1}$).

Table 1 Physical pore parameters of Ni–Co PBA particles produced with the conventional stirring-mix method and continuous flow microreactor

Samples	S_{BET} ($\text{m}^2 \text{g}^{-1}$)	Median pore width ^a (Å)	Pore volume ^b ($\text{cm}^3 \text{g}^{-1}$)	Ref.
NiCoP Cubes	32.90	—	—	44
Ni–Co PBA	11.09	13.8	0.014	45
Ni–Co PBA	114	—	0.038	46
Ni–Co PBA-1#	77.36	7.24	0.20	This work
Ni–Co PBA-1#-2	210.54	7.4	0.26	This work
Ni–Co PBA-1#-6	223.5	6.52	0.27	This work
Ni–Co PBA-1#-10	85.12	8.72	0.25	This work
Ni–Co PBA-1#-14	74.19	9.24	0.20	This work
Ni–Co PBA-2#	95.04	7.28	0.24	This work
Ni–Co PBA-2#-2	106.1	8.83	0.76	This work
Ni–Co PBA-2#-6	111.47	7.26	0.24	This work
Ni–Co PBA-2#-10	208.93	8.84	1.25	This work
Ni–Co PBA-2#-14	245.68	7.03	0.73	This work
Ni–Co PBA-3#	93.33	7.55	0.41	This work
Ni–Co PBA-3#-2	113.76	8.14	0.77	This work
Ni–Co PBA-3#-6	139.34	8.15	0.41	This work
Ni–Co PBA-3#-10	226.32	7.09	0.71	This work
Ni–Co PBA-3#-14	250.05	7.09	1.13	This work

^a Obtained by the Horvath–Kawazoe method. ^b Total pore volume calculated from nitrogen adsorption at saturated pressure.

outstanding quality. It should be noted that there is a certain correlation between the specific surface area and particle size.^{47–49} There is a negative correlation between particle size and specific surface area. The particles with smaller sizes are more effective in enhancing the specific surface area. The above characterizations demonstrate that Ni–Co PBA can be expeditiously produced in a continuous flow microreactor and the particle size can be efficiently controlled by adjusting feed flow rates and concentration of raw materials.

In order to achieve mass production, three times concentration of the raw materials is used to synthesize Ni–Co PBA in a microreactor. Meanwhile, we continue to adjust the feed flow rate of the microreactor for further experiments to obtain Ni–Co PBA with stable particle size. As presented in SEM images of Fig. 9, the particle size of the Ni–Co PBA is 195, 172, 168, 175, 166 and 169 nm at feed flow rates of 10, 20, 25, 30, 35 and 40 mL min^{-1} , respectively. Notably, the particle size of Ni–Co PBA particles is constant ($165 \pm 10 \text{ nm}$) at feed flow rates $> 20 \text{ mL min}^{-1}$.

The relationship between feed flow rates and particle size is investigated to study mixing performance in a continuous flow microreactor. The Reynolds number (Re) is calculated according to the following formula:

$$\text{Re} = \frac{\rho UL}{\mu} \quad (1)$$

ρ is the density of the fluid (1.03 g cm^{-3}), U is the velocity of the liquid, L is the characteristic distance (pipe diameter = $940 \mu\text{m}$), and μ is the dynamic viscosity of the fluid. The dynamic viscosity of the Ni–Co PBA suspension is measured to be $1.24 \times 10^{-3} \text{ Pa s}$ at room temperature.

U is calculated as follows:

$$U = \frac{4V_{\text{total}}}{\pi L^2} \quad (2)$$

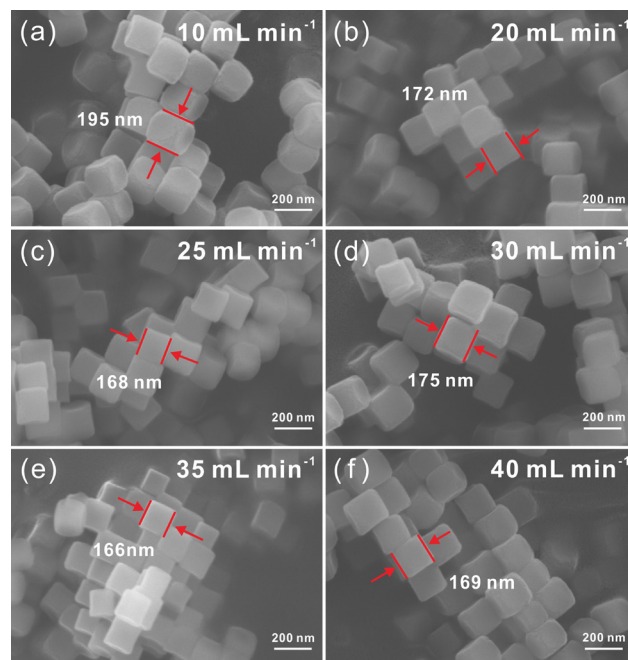


Fig. 9 The SEM images of Ni–Co PBA nanoparticles obtained at feed flow rates of (a) 10 mL min^{-1} , (b) 20 mL min^{-1} , (c) 25 mL min^{-1} , (d) 30 mL min^{-1} , (e) 35 mL min^{-1} and (f) 40 mL min^{-1} in the continuous flow microreactor technology. (The same experiment was carried out 30 times under the same conditions.)

V_{total} is the total flow rate of the raw materials ($V_{\text{total}} = 2\nu$). As shown in Fig. 10, when $\text{Re} < 783$, the particle size decreases with increasing flow rates. It demonstrates that increasing the shear force between the fluids of raw materials improves the mixing performance. The mixing in microchannels provides optimum mixing performance in the Re range. The higher the Re, the stronger the effect. The particle size at $783 < \text{Re} < 1567$ remained unchanged, proving adequately high mixing

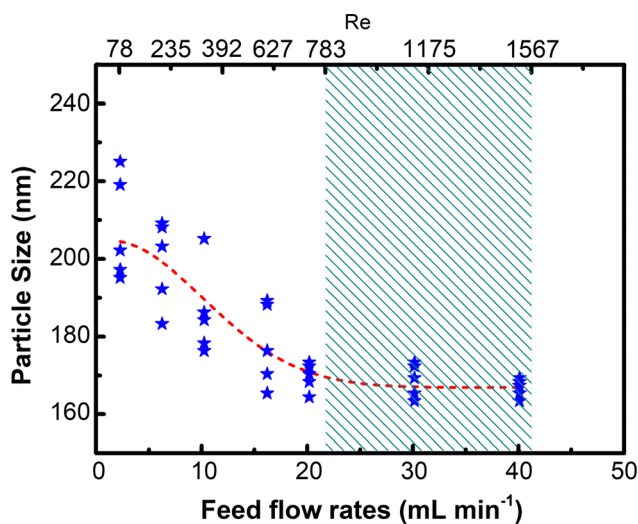


Fig. 10 Relationship between feed flow rates and particle size of resultant Ni–Co PBA-3#-X ($X = 2, 4, 6, 8, 10, 12, 14$ and 16 mL min^{-1}) particles. Re was calculated from flow rates.

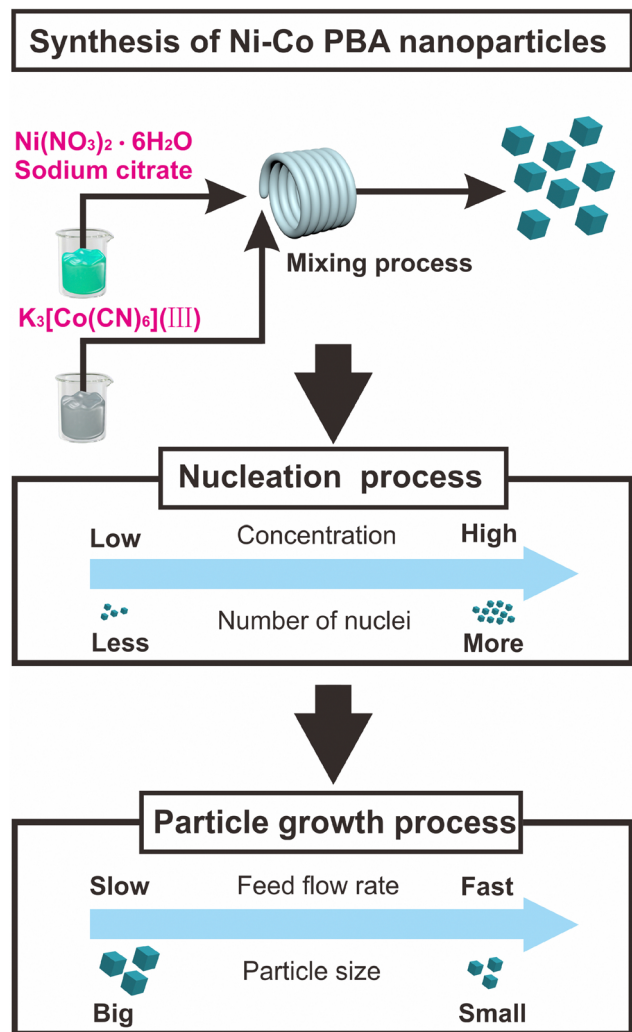


Fig. 11 Schematic control of nucleation process and particle growth process of Ni-Co PBA nanoparticle synthesis process.

performance for mixing raw materials. The result is consistent with the SEM images (Fig. 9). The particle size of Ni-Co PBA nanoparticles at feed flow rates of 20 mL min⁻¹ to 40 mL min⁻¹ is 165 ± 10 nm among the trials.

Furthermore, the space-time yield (STY) and production rate of Ni-Co PBA synthesized in a microreactor are greatly improved compared with the conventional stirring-mix method. We calculate the space-time yield (STY) and production rate of Ni-Co PBA synthesized by the two methods. The STY calculation formula for flow and batch synthesis is as follows:⁵⁰

$$STY = \frac{m_{\text{Ni-Co PBA}}}{V_{\text{solution}}\tau} \times 1.44 \times 10^6 \quad (3)$$

$m_{\text{Ni-Co PBA}}$ is the weight of the product (g), V_{solution} is the total volume of the mixture (mL), and τ is the reaction time (min) plus the crystallization time. When the feed flow rate is 30 mL min⁻¹, the STY of Ni-Co PBA-3#-30 is up to 471 kg m⁻³ d⁻¹, which is much higher than conventional stirring-mix method values of 4.42 kg m⁻³ d⁻¹. And the corresponding production rates are 518.4 and 0.53 g d⁻¹, respectively.

Based on these results, the mechanism for the synthesis of Ni-Co PBA through a fast-mixing reaction is proposed (Fig. 11). Ni(NO₃)₂·6H₂O, sodium citrate and K₃[Co(CN)₆](III) are mixed at room temperature after being pumped into the microreactor system. Initially, Ni-Co PBA seed complexes are formed. As the increasing concentration of raw materials accelerates the nucleation rate, more seed nanoparticles are formed which is expected to lead to a smaller final nanoparticle size. These formed nuclei can grow for a further period of time until the reaction reaches equilibrium. Once the reaction has reached equilibrium crystal growth can no longer be sustained. Therefore, the nucleation process can be controlled by changing the concentration of raw materials, that is, a higher concentration produces more nuclei, leading to smaller particles. At the same time, the feed flow rates have an influence on the particle growth process, and the feed flow rate increases to a certain extent, and the particle grows steadily. We can control the particle size of Ni-Co PBA by varying the mixing performance, concentration and feed flow rates. An excellent procedure for the preparation of small particle size Ni-Co PBA is rapid mixing with a suitable concentration at a high feed flow rate. We look forward that the microreactor can be used for the rapid synthesis of other MOFs, because it can effectively control the mixing performance.

4. Conclusions

In this paper, Ni-Co PBA nanoparticles were synthesized *via* a microreactor and the effect of the feed flow rate and the concentration of raw materials on their mixing performance was investigated. Remarkably, the microreactor exhibited prominent mixing performance and synthesized Ni-Co PBA with a narrow size distribution. The nucleation process and the particle growth process are controlled by adjusting feed flow rates and the concentration of raw materials. On the one hand, the particle size of Ni-Co PBA can be easily tuned by simply controlling the feed flow rates. The particle size decreases with increasing flow rates at $Re < 783$. When the feed flow rate is 20 mL min⁻¹ to 40 mL min⁻¹ ($783 < Re < 1567$), the particle size is kept as small as 165 ± 10 nm. On the other hand, the high concentration of raw materials could decrease the particle size in the particle growth process. Ultimately, the experimental phenomenon demonstrates that the changes in experimental conditions only affect the particle size and size distributions. Owing to the continuous flow microreactor strategy, the preparation of Ni-Co PBA particles in the microreactor helps achieve the goal of large-scale production, and the space-time yield is up to 471 kg m⁻³ d⁻¹. These results will attract more attention to the development of simple methods to fabricate MOFs with tunable particle sizes and application-specific functionalities.

Author contributions

Huanhuan Wang: conceptualization, methodology, writing – original draft preparation and writing – editing. Qi Qu: writing – reviewing, data curation. Zhiming Liu: data curation. Yan He:

investigation, supervision, funding acquisition. Jiangshan Gao: investigation, funding acquisition.

Conflicts of interest

There are no conflicts of interest to declare.

Acknowledgements

This work was supported by the National Natural Science Foundation of China (No. 52176076, 51676103), Taishan Scholar Project of Shandong Province, China (No.ts20190937) and Natural Science Foundation of Shandong Province, China (No. ZR2021QE007).

References

- 1 P. M. Bhatt, V. Guillermin, S. J. Datta, A. Shkurenko and M. Eddaoudi, Topology meets reticular chemistry for chemical separations: MOFs as a case study, *Chem*, 2020, **6**, 1613–1633.
- 2 P. Miao, J. X. Chen, Y. S. Tang, K. J. Chen and J. Kong, Highly efficient and broad electromagnetic wave absorbers tuned via topology-controllable metal-organic frameworks, *Sci. China Mater.*, 2020, **63**, 2050–2061.
- 3 W. X. Zhang, H. Song, Y. Cheng, C. Liu, C. H. Wang, M. A. N. Khan, H. Zhang, J. Z. Liu, C. Z. Yu, L. J. Wang and J. S. Li, Core-shell prussian blue analogs with compositional heterogeneity and open cages for oxygen evolution reaction, *Adv. Sci.*, 2019, **6**, 1801901.
- 4 Y. Feng, X. Y. Yu and U. Paik, Nickel cobalt phosphides quasi-hollow nanocubes as an efficient electrocatalyst for hydrogen evolution in alkaline solution, *Chem. Commun.*, 2016, **52**, 1633–1636.
- 5 X. Y. Yu, Y. Feng, Y. Jeon, B. Guan, X. W. Lou and U. Paik, Formation of Ni-Co-MoS₂ nanoboxes with enhanced electrocatalytic activity for hydrogen evolution, *Adv. Mater.*, 2016, **28**, 9006–9011.
- 6 J. S. Gao, H. H. Wang, Y. Zhou, Z. M. Liu and H. Yan, Self-template and in-situ synthesis strategy to construct MnO₂/Mn₃O₄@Ni-Co/GC nanocubes for efficient microwave absorption properties, *J. Alloys Compd.*, 2022, **892**, 162151.
- 7 B. Nayebe, K. P. Niavol, B. Nayebe, S. Y. Kim, K. T. Nam, H. W. Jang, R. S. Varma and M. Shokouhimehr, Prussian blue-based nanostructured materials: Catalytic applications for environmental remediation and energy conversion, *Mol. Catal.*, 2021, **514**, 111835.
- 8 S. T. Gao, Y. C. Zhang, H. L. Xing and H. X. Li, Controlled reduction synthesis of yolk-shell magnetic@void@C for electromagnetic wave absorption, *Chem. Eng. J.*, 2020, **387**, 124149.
- 9 J. S. Gao, S. L. Li, H. H. Wang, Y. Zhou, L. Y. Zhang, Z. M. Liu and Y. He, Carbon nanotubes aerogels dispersed by thermal excitation on Ni Foam@NiCo₂O₄ nanoneedles with enhanced properties for supercapacitor, *J. Alloys Compd.*, 2021, **861**, 157963.
- 10 J. S. Gao, Z. M. Liu, Y. Lin, Y. Z. Tang, T. T. Lian and Y. He, NiCo₂O₄ nanofeathers derived from prussian blue analogues with enhanced electrochemical performance for supercapacitor, *Chem. Eng. J.*, 2020, **388**, 124368.
- 11 X. Y. Wu, Y. Ru, Y. Bai, G. X. Zhang, Y. X. Shi and H. Pang, PBA composites and their derivatives in energy and environmental applications, *Coord. Chem. Rev.*, 2022, **451**, 214260.
- 12 S. Andonova, S. S. Akbari, F. Karadaş, I. Spassova, D. Paneva and K. Hadjiivanov, Structure and properties of KNi-hexacyanoferrate prussian blue analogues for efficient CO₂ capture: Host-guest interaction chemistry and dynamics of CO₂ adsorption, *J. CO₂ Util.*, 2021, **50**, 101593.
- 13 D. Su and G. Kaur, A comprehensive review on synthetic approaches for metal-organic frameworks: From traditional solvothermal to greener protocols, *Polyhedron*, 2020, **193**, 114897.
- 14 C. Q. Wang, G. J. Ren, K. F. Wei, D. H. Liu, T. T. Wu, J. L. Jiang, J. F. Qian and Y. C. Pan, Improved dispersion performance and interfacial compatibility of covalent-grafted MOFs in mixed-matrix membranes for gas separation, *Green Chem. Eng.*, 2021, **2**, 86–95.
- 15 S. Z. Hu, T. Huang, N. Zhang, Y. Z. Lei and Y. Wang, Chitosan-assisted MOFs dispersion via covalent bonding interaction toward highly efficient removal of heavy metal ions from wastewater, *Carbohydr. Polym.*, 2021, **277**, 118809.
- 16 J. T. Li, J. F. Zheng, X. Cheng, G. H. Yue and X. T. Luo, NiFeP nanocages embedded in melamine sponge derived nitrogen doped porous carbon foam as an efficient oxygen evolution electrocatalyst, *J. Solid State Chem.*, 2019, **278**, 120881.
- 17 R. L. M. Robinson, I. Lynch, W. Peijnenburg, J. Rumble, F. Klaessig, C. Marquardt, H. Rauscher, T. Puzyn, R. Purian, C. Åberg, S. Karcher, H. Vriens, P. Hoet, M. D. Hoover, C. O. Hendren and S. L. Harper, How should the completeness and quality of curated nanomaterial data be evaluated?, *Nanoscale*, 2016, **8**, 9919–9943.
- 18 C. Portier, T. Vigh, G. D. Pretoro, J. Leys, D. Klingeleers, T. D. Beer, C. Vervaet and V. Vanhoorne, Continuous twin screw granulation: impact of microcrystalline cellulose batch-to-batch variability during granulation and drying-A QbD approach, *Int. J. Pharm.*, 2021, **3**, 100077.
- 19 H. Yoo, H. E. Byun, D. H. Han and J. H. Lee, Reinforcement learning for batch process control: Review and perspectives, *Annu. Rev. Control*, 2021, **52**, 108–119.
- 20 F. Grimaldi, M. Pucciarelli, A. Gavrilidis, P. Dobson and P. Lettieri, Anticipatory life cycle assessment of gold nanoparticles production: Comparison of milli-continuous flow and batch synthesis, *J. Cleaner Prod.*, 2020, **269**, 122335.
- 21 M. Periyasamy, A. Saha, S. Sain and M. Mandal, A comparative structural and photocatalytic study on SnO₂ nanoparticles fabricated in batch reactor and microreactor, *J. Environ. Chem. Eng.*, 2020, **8**, 104604.
- 22 A. Schejn, M. Frégnaux, J. M. Commenge, L. Balan, L. Falk and R. Schneider, Size-controlled synthesis of ZnO quantum dots in microreactors, *Nanotechnology*, 2014, **25**, 145606.
- 23 Z. Yao, X. Xu, Y. L. Dong, X. Liu, B. Yuan, K. Wang, K. Cao and G. S. Luo, Kinetics on thermal dissociation and

- oligomerization of dicyclopentadiene in a high temperature & pressure microreactor, *Chem. Eng. Sci.*, 2020, **228**, 115892.
- 24 G. Tofighi, A. Gaur, D. E. Doronkin, H. Lichtenberg, W. Wang, D. Wang, G. Rinke, A. Ewinger, R. Dittmeyer and J. D. Grunwaldt, Microfluidic synthesis of ultrasmall aupd nanoparticles with a homogeneously mixed alloy structure in fast continuous flow for catalytic applications, *J. Phys. Chem. C*, 2018, **122**, 1721–1731.
 - 25 H. Yang, E. M. Akinoglu, L. J. Guo, M. L. Jin, G. F. Zhou, M. Giersig, L. L. Shui and P. Mulvaney, A PTFE helical capillary microreactor for the high throughput synthesis of monodisperse silica particles, *Chem. Eng. J.*, 2020, **401**, 126063.
 - 26 Y. Song, J. A. Song, M. J. Shang, W. H. Xu, S. Liu, B. Y. Wang, Q. H. Lu and Y. H. Su, Hydrodynamics and mass transfer performance during the chemical oxidative polymerization of aniline in microreactors, *Chem. Eng. J.*, 2018, **353**, 769–780.
 - 27 R. K. Jiang, X. Xue, F. Zhao, W. P. Zhu, M. J. Shang, Y. H. Su, Y. F. Xu and X. H. Qian, Process parameter and kinetic study for the azidation of a zidovudine intermediate with sodium azide in microreactors, *Chem. Eng. J.*, 2022, **429**, 132207.
 - 28 K. B. Goh, Z. Li, X. Chen, Q. M. Liu and T. Wu, Reaction-diffusion model to quantify and visualize mass transfer and deactivation within core-shell polymeric microreactors, *J. Colloid Interface Sci.*, 2021, **608**, 1999–2008.
 - 29 N. A. Jose, H. C. Zeng and A. A. Lapkin, Scalable and precise synthesis of two-dimensional metal organic framework nanosheets in a high shear annular microreactor, *Chem. Eng. J.*, 2020, **388**, 124133.
 - 30 J. Zhang, Y. H. Wang and F. Wang, Microreactor-assisted synthesis of a nickel-based infinite coordination polymer and its application in the selective adsorption of alcohols, *Inorg. Chem. Commun.*, 2019, **109**, 107566.
 - 31 S. J. Tai, W. Q. Zhang, J. S. Zhang, G. X. Luo, Y. Jia, M. L. Deng and Y. Ling, Facile preparation of UiO-66 nanoparticles with tunable sizes in a continuous flow microreactor and its application in drug delivery, *Microporous Mesoporous Mater.*, 2016, **220**, 148–154.
 - 32 M. Z. Zhang, Z. Q. Yu, Z. C. Sun, A. J. Wang, J. Zhang, Y. Y. Liu and Y. Wang, Continuous synthesis of ZIF-67 by a microchannel mixer: A recyclable approach, *Microporous Mesoporous Mater.*, 2021, **327**, 111423.
 - 33 A. Polyzoidis, M. Schwarzer, S. Loebbecke and C. G. Piscopo, Continuous synthesis of UiO-66 in microreactor: Pursuing the optimum between intensified production and structural properties, *Mater. Lett.*, 2017, **197**, 213–216.
 - 34 A. Toyota, H. Nakamura, H. Ozono, K. Yamashita, U. Masato and H. Maeda, Combinatorial synthesis of cdse nanoparticles using microreactors, *J. Phys. Chem. C*, 2010, **114**, 7527–7534.
 - 35 P. Reuse, A. Renken, K. Haas-Santo, O. Görke and K. Schubert, Hydrogen production for fuel cell application in an autothermal micro-channel reactor, *Chem. Eng. J.*, 2004, **101**, 133–141.
 - 36 J. S. Gao, Y. Zhou, Z. M. Liu, H. H. Wang and Y. He, NiCo-Se nanoparticles encapsulated n-doped cnts derived from prussian blue analogues for high performance supercapacitors, *Electrochim. Acta*, 2022, **411**, 140064.
 - 37 D. Yamamoto, T. Maki, S. Watanabe, H. Tanak, M. T. Miyahara and K. Mae, Synthesis and adsorption properties of ZIF-8 nanoparticles using a micromixer, *Chem. Eng. J.*, 2013, **227**, 145–150.
 - 38 O. Kolmykov, J. M. Commenge, H. Alem, E. Girod, K. Mozet, G. Medjahdi and R. Schneider, Microfluidic reactors for the size-controlled synthesis of ZIF-8 crystals in aqueous phase, *Mater. Des.*, 2017, **122**, 31–41.
 - 39 R. J. Dombrowski, C. M. Lastoskie and D. R. Hyduke, The Horvath-Kawazoe method revisited, *Colloids Surf., A*, 2001, **187**, 23–39.
 - 40 S. Watanabe, Y. Asahi, H. Omura, K. Mae and M. T. Miyahara, Flow microreactor synthesis of gold nanoshells and patchy particles, *Adv. Powder Technol.*, 2016, **27**, 2335–2341.
 - 41 H. B. Yu, M. D. Wang, J. H. Zhou, B. Yuan, J. Luo, W. Wu, Z. Chen and R. X. Yu, Microreactor-assisted synthesis of α -alumina nanoparticles, *Ceram. Int.*, 2020, **46**, 13272–13281.
 - 42 T. Jaouhari, F. Zhang, T. Tassaing, S. Fery-Forgues, C. Aymoniera, S. Marrea and A. Erriguible, Process intensification for the synthesis of ultra-small organic nanoparticles with supercritical CO₂ in a microfluidic system, *Chem. Eng. J.*, 2020, **397**, 125333.
 - 43 C. M. Lastoskie, A modified Horvath-Kawazoe method for micropore size analysis, *Stud. Surf. Sci. Catal.*, 2000, **128**, 475–484.
 - 44 D. Li, C. J. Zhou, Y. Y. Xing, X. L. Shi, W. X. Ma, L. H. Li, D. L. Jiang and W. D. Shi, Oxygen-doped hollow, porous nicop nanocages derived from Ni-Co prussian blue analogs for oxygen evolution, *Chem. Commun.*, 2021, **57**, 8158–8161.
 - 45 W. Wang, J. Zhong, Z. Zhu, A. Gao, F. Yi, J. Ling, J. Hao and D. Shu, Hollow NiCoP nanocubes derived from a Prussian blue analogue self-template for high-performance supercapacitors, *J. Alloys Compd.*, 2022, **893**, 162344.
 - 46 C. Marquez, F. G. Cirujano, C. Van Goethem, I. Vankelecom, D. De Vos and T. De Baerdemaeker, Tunable Prussian blue analogues for the selective synthesis of propargylamines through A³ coupling, *Catal. Sci. Technol.*, 2018, **8**, 2061–2065.
 - 47 J. W. Bullard, Q. Jin and K. A. Snyder, How do specific surface area and particle size distribution change when granular media dissolve, *Chem. Eng. J.*, 2021, **406**, 127098.
 - 48 S. Sompech, A. Srion and A. Nuntiya, The effect of ultrasonic treatment on the particle size and specific surface area of LaCoO₃, *Procedia Eng.*, 2012, **32**, 1012–1018.
 - 49 M. Mosharraf and C. Nyström, The effect of particle size and shape on the surface specific dissolution rate of micro-sized practically insoluble drugs, *Int. J. Pharm.*, 1995, **122**, 35–47.
 - 50 C. X. Duan, Y. Yu, F. E. Li, Y. Wu and H. X. Xi, Ultrafast room-temperature synthesis of hierarchically porous metal-organic frameworks with high space-time yields, *CrystEngComm*, 2020, **22**, 2675–2680.